Scientific Research Publishing

Open Journal of Applied Sciences, 2025, 15(1), 352-373
https://www.scirp.org/journal/ojapps
ISSN Online: 2165-3925
ISSN Print: 2165-3917

Design and Optimization of Terracotta Tube-Based Direct Evaporative Cooling Exchanger: An Analytical Approach to Heat and Mass Transfer

Windnigda Zoungrana[1,2*], Makinta Boukar[1], Ousmane Coulibaly[2], Guy Christian Tubreoumya[2], Antoine Bere[2]

[1]Laboratoire d'Energétique, d'Electronique, d'Electrotechnique, d'Automatique et d'informatique Industrielle, Université Abdou Moumouni, Niamey, Niger
[2]Laboratoire de Physique et de Chimie de l'Environnement, Université Joseph Ki Zerbo, Ouagadougou, Burkina Faso
Email: *windnigda@gmail.com

How to cite this paper: Zoungrana, W., Boukar, M., Coulibaly, O., Tubreoumya, G.C. and Bere, A. (2025) Design and Optimization of Terracotta Tube-Based Direct Evaporative Cooling Exchanger: An Analytical Approach to Heat and Mass Transfer. *Open Journal of Applied Sciences*, **15**, 352-373.
https://doi.org/10.4236/ojapps.2025.151022

Received: December 29, 2024
Accepted: January 27, 2025
Published: January 30, 2025

Abstract

This study develops an analytical model to evaluate the cooling performance of a porous terracotta tubular direct evaporative heat and mass exchanger. By combining energy and mass balance equations with heat and mass transfer coefficients and air psychrometric correlations, the model provides insights into the impact of design and operational parameters on the exchanger cooling performance. Validated against an established numerical model, it accurately simulates cooling behavior with a Root Mean Square Deviation of 0.43 - 1.18˚C under varying inlet air conditions. The results show that tube geometry, including equivalent diameter, flatness ratio, and length significantly influences cooling outcomes. Smaller diameters enhance wet-bulb effectiveness but reduce cooling capacity, while increased flatness and length improve both. For example, extending the flatness ratio of a 15 mm diameter, 0.6 m long tube from 1 (circular) to 4 raises the exchange surface area from 0.028 to 0.037 m^2, increasing wet-bulb effectiveness from 60% to 71%. Recommended diameters range from 5 mm for tubes under 0.5 m to 1 cm for tubes 0.5 to 1 m in length. Optimal air velocities depend on tube length: 1 m/s for tubes under 0.8 m, 1.5 m/s for lengths of 0.8 to 1.2 m, and up to 2 m/s for longer tubes. This model offers a practical alternative to complex numerical and CFD methods, with potential applications in cooling tower optimization for thermal and nuclear power plants and geothermal heat exchangers.

Keywords

Analytical Modeling, Porous Terracotta Tube, Direct Evaporative Cooling, Heat and Mass Exchanger, Performance Optimization

1. Introduction

Simultaneous heat and mass transfer in porous media plays a critical role in diverse scientific and engineering applications, including evaporative cooling (EC) [1]-[3]. EC technology stands out as one of the promising alternatives to conventional vapor compression air conditioning systems [4]. It is recognized for its resource-saving and eco-friendly nature, owing to its exceptional cooling efficiency and the use of porous media as an efficient heat and mass transfer medium.

The wet medium is an essential component in an EC system. It is usually made of a porous material with a large microscopic surface area and capacity to hold liquid water. The selection of wet media materials would depend on the application, effectiveness, availability, cost, safety, and environmental factors [5]. Various cooling pad materials, such as wood straw, PVC, metal meshes, coconut fibers, felt, and fiber-polymer composites, have been explored to enhance water absorption and reduce pressure drop [6]-[8]. However, issues like weak antibacterial properties [9], rapid decay, maintenance challenges of organic pads [10] [11], and the high costs of synthetic pads have driven researchers to explore alternative materials for improved efficiency and durability.

Porous ceramics have emerged as an alternative pad material for evaporative cooling applications due to their water-soaking capacity, antibacterial ability, broad availability, and cost-effectiveness [12]. Their high porosity, large surface area, and moderate thermal conductivity enhance performance by improving surface wettability, maximizing air-water contact, and serving as a water reservoir. This enables intermittent water spraying, reducing pump energy consumption. Precise control of pore size and porosity further makes them adaptable to diverse applications [13].

Among the various shapes of porous ceramic media, hollow terracotta tubes arranged to form a bundle have also gained popularity as an evaporative cooling medium. Most research in Terracotta Tubular Evaporative Cooling (TT-EC) focuses on cross-flow indirect and semi-indirect configurations [14]. Amer and Boukhanouf [15] conducted an experimental investigation to evaluate the effect of various operational conditions on a novel heat pipe and ceramic tube-based evaporative cooler. The thermal comfort provided by a combined recovery equipment consisting of a terracotta semi-IEC and a heat pipe device (HP) was investigated by Martín *et al*. [16]. A porous ceramic made semi-IEC was designed, manufactured, and tested by Gómez *et al*. [17]. The device can act as a heat recovery system in tropical environments where the system yields a decrease in supply air humidity. Except for semi-indirect and indirect EC, the porous ceramic has also

been used in direct evaporative cooler (DEC) as filler [18]. Chen *et al*. [19] experimentally studied porous terracotta pipes with high water-sucking ability for an evaporative cooling wall.

Numerical modeling has been widely applied to examine the effects of various parameters, including inlet air psychrometric properties, fluid flow conditions, and pad geometry, on heat and mass transfer processes within a wet tube channel. Mechergui *et al*. [20] explored evaporation in laminar flow, revealing that wall temperature, heat flux, inlet air temperature, and humidity significantly affect outlet humidity, and temperature profiles. Kassim *et al*. [21] and Cherif *et al*. [22] identified air velocity, temperature, and humidity as the most critical factors in vertical channel systems. Cossali and Tonini [23] highlighted the necessity of incorporating variable thermo-physical properties in heat and mass transfer models, revealing discrepancies of 8–30% when constant properties are used. Channel geometry has also been studied in depth. Adam *et al*. [24] concluded that, for optimal performance in moderately humid climates, duct lengths should range from 0.6 to 1.0 meters, channel widths from 0.3 to 0.5 meters, and channel gaps from 0.004 to 0.008 meters. Similarly, Sun *et al*. [25] showed that reducing the equivalent diameter of porous ceramic pipes in indirect evaporative coolers lowers outlet temperatures and improves wet-bulb effectiveness. These findings underscore the importance of both operating conditions and geometric parameters in optimizing evaporative cooling performance.

Existing studies have largely focused on round tubular EC, but flat tubular variants, which offer notable advantages, remain less explored. Flat tubular ECs provide superior wetting characteristics and better water film formation [26]. They also create more compact systems compared to round tubular configurations [27]. Liu *et al*. [28] developed a direct-expansion ice thermal storage system that incorporates a multi-channel flat-tubular evaporator, analyzing key factors to enhance system performance. Windnigda *et al*. [29] explored the impact of tube geometric parameters on the cooling performance of Terracotta Flat Tubular Heat and Mass Exchangers through experimental testing and numerical simulations. These findings underscore the potential of flat tubular ECs for advanced and efficient cooling applications.

Significant progress has been made in understanding heat and mass transfer in wet tube channels. Theoretically, when hot fluid flows within a wet tube, it heats its interior surface. The water film covering the tube's interior evaporates into the air passing through. The air cools down while getting moisture. This process involves both sensible and latent heat transfer. The theory of tubular Evaporative Cooling (EC) is well-established in process engineering. Advances in experimental techniques, numerical simulations, and high-performance computation (HPC) methods like CFD have enhanced predictions of these interactions. However, these methods entail substantial costs and time investments, particularly when applied to iterative optimization and real-time control purposes. More recently, practical models based on statistical correlations [30] [31] and emerging

Artificial Neural Network (ANN) methods [32]-[35] have been developed. However, correlations are typically developed for specific configurations, operating ranges, and environmental conditions. Applying them beyond these conditions can lead to significant inaccuracies. Furthermore, they require extensive experimental data to be accurate and reliable, and may not perform well when applied to new systems or design purposes.

To address these research gap, this study develops an analytical model to examine the effects of geometric and operating parameters on the cooling performance of a porous ceramic tube heat and mass exchanger. This analytical approach seeks to enhance the understanding and optimization of EC systems employing porous ceramic tubes, ultimately promoting the development of more efficient and sustainable air-conditioning systems.

2. Description of the Porous Ceramic Tube Heat and Mass Exchanger

2.1. Geometric Parameters

The porous ceramic evaporator used in this study is a hollow terracotta tube with a flat geometry, as shown in Figure 1.

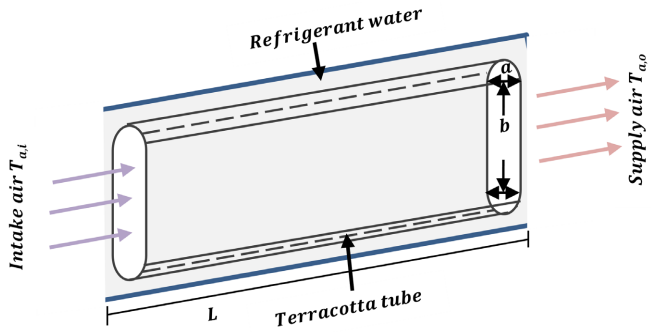

Figure 1. Porous terracotta tube heat and mass exchanger geometry.

The geometry of this heat and mass exchanger is defined by three key parameters: the tube's short axis (a), long axis ($a+b$), and length (L). Additional parameters, including perimeter (p), cross-sectional area (A_c), exchange surface area (A_w), flatness ratio (R_F), and characteristic length (hydraulic diameter (D_h) or equivalent diameter (D_e), are calculated using specific formulas.

Perimeter

$$p = \pi a + 2b \tag{1}$$

Cross-section area

$$A_c = \frac{a^2\pi}{4} + ab \tag{2}$$

Wet surface area

The wet surface area is computed using Equation (3).

$$A_w = L\left[\pi a + 2b\right] \tag{3}$$

Equivalent diameters

For non-circular tubes, the equivalent diameter is typically used in Reynolds number calculations instead of hydraulic diameter [36]:

$$D_h = \frac{4A_c}{P} \tag{4}$$

$$D_e = \sqrt{\frac{4A_c}{\pi}} \tag{5}$$

Tube flatness ratio

The tube flatness ratio is defined as the ratio of the tube's long axis to its short axis:

$$R_F = \frac{a+b}{a} \tag{6}$$

Given the equivalent diameter and flatness ratio, the values of a and b can be determined by solving the following equation:

$$A_c = \frac{\pi D_e^2}{4} = \frac{a^2\pi}{4} + ab \tag{7}$$

$$\text{For}: R_F = 1 \to b = 0 \text{ and } a = D_e \to \text{this correspond to the circular tube}.$$

$$\text{For}: R_F = 2 \to b = a \text{ and } a = D_e\sqrt{(\pi/4)/(1+\pi/4)}.$$

$$\text{For}: R_F = 3 \to b = 2a \text{ and } a = D_e\sqrt{(\pi/4)/(2+\pi/4)}.$$

$$\text{For}: R_F = 4 \to b = 3a \text{ and } a = D_e\sqrt{(\pi/4)/(3+\pi/4)}.$$

The influence of the flatness ratio on the hydraulic diameter and the tube exchange surface area is shown in Table 1. It is evident that the equivalent diameter is larger than the hydraulic diameter with increasing differences at higher flatness ratios.

Table 1. Influence of flatness ratio on tube hydraulic diameter and perimeter.

Tube flatness	Tube geometric parameters					
	D_e (mm)	a (mm)	b (mm)	P_w (mm)	A_c (mm²)	D_h (mm)
Round (1)	15	15	0	47.12	176.71	15
2	15	9.95	9.95	51.15	176.71	13.82
3	15	7.96	15.93	56.88	176.71	12.43
4	15	6.83	20.50	62.46	176.71	11.32

2.2. Physical Model of the Heat and Mass Exchanger

The physical description of the terracotta tubular heat and mass exchanger is shown in Figure 2. The heat and mass transfer process within the wet tube channel involves a sequence of mechanisms that facilitate air temperature reduction as it flows through the channel. In the wet tube, the inner surface is kept moist,

allowing water to evaporate from this surface into the air flowing through the tube. As the warm air enters the tube, it initiates a transfer of heat from the air to the wetted surface, facilitating the phase change of water from liquid to vapor. This evaporation process absorbs heat from the air (latent heat of vaporization), reducing the air temperature while increasing it moisture content. This cooling effect relies on several factors: the air's initial temperature and humidity, the temperature and moisture of the wetted surface, and the tube geometry.

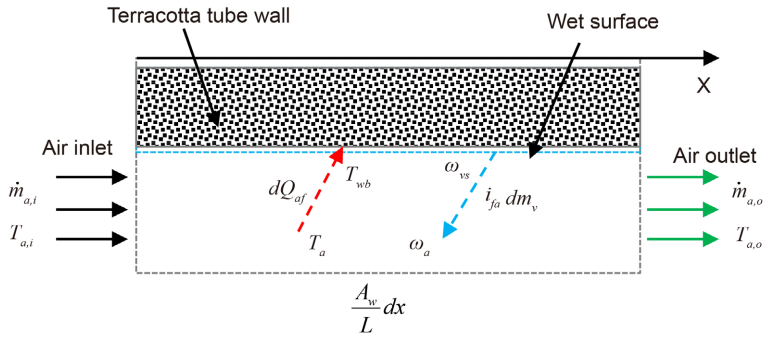

Figure 2. Physical model of the terracotta heat and mass exchanger.

3. Mathematical Model Development

3.1. Simplifying Assumptions

To develop the mathematical model, the following assumptions are made:

- Heat and mass exchange with surroundings are negligible;
- The kinetic energy gain is negligible;
- The potential energy gain is negligible;
- The process is assumed to be under steady-state open system;
- Flow, heat, and mass are to be under a steady state;
- The interior surface of the tube's wall is completely and continuously wet;
- The wet surface temperature is assumed to be identical to the wet bulb temperature of the inlet air;
- No condensation happens in the tube channel;
- All thermo-physical properties of air are temperature-dependent.

3.2. Governing Equations

The heat and mass transfer process in a wet tube channel is governed by energy and mass conservation principles. These equations account for convective heat and mass transfer, evaporation, and variations in air temperature and humidity along the tube.

Mass and Heat Transfer:

- Mass transfer, driven by vapor density gradients:

$$\mathrm{d}m_v = \rho_a h_m \left(\omega_{vs} - \omega_a\right) \frac{A_w}{L} \mathrm{d}x \tag{8}$$

- Heat transfer, driven by temperature gradients:

$$\mathrm{d}Q_{af} = h_a\left(T_a - T_{wb}\right)\frac{A_w}{L}\mathrm{d}x \tag{9}$$

Energy Balance Equation for humid air:

The energy balance describes air temperature changes due to heat and mass transfer:

$$\mathrm{d}\left(\dot{m}_a i_a\right) + \mathrm{d}\left(\dot{m}_v i_v\right) = -\mathrm{d}Q_{af} + i_{vf}\,\mathrm{d}m_v \tag{10}$$

$$i_a \mathrm{d}\dot{m}_a + \dot{m}_a \mathrm{d}i_a + \mathrm{d}m_v \mathrm{d}i_v + i_v \mathrm{d}m_v = -\mathrm{d}Q_{af} + i_{vf}\,\mathrm{d}m_v \tag{11}$$

$$\dot{m}_a\left(c_{pa} + \omega_a c_{pv}\right)\mathrm{d}T_a + \left(i_0 + c_{pv}T_a\right)\mathrm{d}m_v = -\mathrm{d}Q_{af} + \left(i_0 + c_{pv}T_{wb}\right)\mathrm{d}m_v \tag{12}$$

Reformulating and combining terms yields:

$$\frac{\mathrm{d}T_a}{\mathrm{d}x} = -\frac{\left[h_a + c_{pv}\rho_a h_m\left(\omega_{vs} - \omega_a\right)\right]A_w}{\dot{m}_a\left(c_{pa} + \omega_a c_{pv}\right)L}\left(T_a - T_{wb}\right) \tag{13}$$

Mass Transfer Equation for humid air:

This equation accounts for the increase in air humidity due to water vapor absorption:

$$\dot{m}_a \mathrm{d}\omega_a = \mathrm{d}m_v \tag{14}$$

$$\frac{\mathrm{d}\omega_a}{\mathrm{d}x} = \frac{A_w \rho_a h_m}{L\dot{m}_a}\left(\omega_{vs} - \omega_a\right) \tag{15}$$

Energy Balance Equation at the wet surface:

In adiabatic processes, the convective heat transfer from the air to the wet surface equals the latent heat for water evaporation. In terms of the heat transfer and mass transfer coefficients, this equation can be expressed as:

$$h_a\left(T_a - T_{wb}\right) = \rho_a h_m i_{fg}\left(\omega_{vs} - \omega_a\right) \tag{16}$$

For temperatures between 0 - 180˚C, the latent heat of vaporization can be approximated as [37]:

$$i_{fg} = 2501.6 - 2.65T_f\ \left(\mathrm{kJ}\cdot\mathrm{kg}^{-1}\right) \tag{17}$$

3.3. Analytical Model Development

Equations (13) & (16) are combined and integrated to obtain an analytical solution:

$$\frac{h_a A_w}{\dot{m}_a\left(c_{pa} + c_{pv}\omega_{vs}\right)} + \ln\left[\frac{T_{a,o} - T_{wb}}{T_{a,i} - T_{wb}}\right] = \left(1 + Le^{\frac{2}{3}}\right)\ln\left[\frac{i_{fg} + c_{pv}\left(T_{a,o} - T_{wb}\right)}{i_{fg} + c_{pv}\left(T_{a,i} - T_{wb}\right)}\right] \tag{18}$$

where Le represents number:

$$Le_f = \frac{h_a}{\rho_a\left(c_{pa} + c_{pv}\omega_{vs}\right)h_m} = Le^{\frac{2}{3}} \tag{19}$$

If the exchange surface area is known, the outlet temperature can be solved iteratively using a computer program.

On the other hand, Equation (15) is integrated to obtain the specific humidity

of the outlet air:

$$\int_{\omega_{a,i}}^{\omega_{a,o}} \frac{-\mathrm{d}\omega_a}{\omega_{vs}-\omega_a} = -\int_0^L \frac{A\rho_a h_m}{L\dot{m}_a}\mathrm{d}x \tag{20}$$

$$\omega_{a,o} = \omega_{a,i} + \left(\omega_{vs}-\omega_{a,i}\right)\left(1-\exp\left[-\frac{A\rho_a h_m}{\dot{m}_a}\right]\right) \tag{21}$$

The moisture content of the saturated air (ω_{vs}) is evaluated at the wet bulb temperature using Equation (22):

$$\omega_{vs} = \frac{0.622\times P_{sat}}{101325-P_{sat}} \tag{22}$$

where saturation pressure (P_{sat}) is expressed by Equation (23) [37]:

$$P_{sat} = 10^5 \times \exp\left\{\left[12.1929 - \frac{4109.1}{\left(T_{wb}+273.15\right)-35.50}\right]\right\} \tag{23}$$

The relative humidity is computed from the specific humidity of the outlet air using Equation (24) [38]:

$$\varnothing = \frac{100\times P_{atm}\omega_{a,o}}{P_{sat}\times\left(0.622+\omega_{a,o}\right)} \tag{24}$$

where the saturation pressure (P_{sat}) are evaluated at the outlet air temperature.

3.4. Performance Parameters

The Wet-bulb Effectiveness (ε_{wb}) is calculated using Equation (25) [39]:

$$\varepsilon_{wb} = \frac{T_{a,i}-T_{a,o}}{T_{a,i}-T_{wb}} \tag{25}$$

where the wet bulb temperature can be computed by Equation (26) [38].

$$T_{wb} = 2.265\times\left[1.97+\left(4.3\times T_{db,i}\right)+\left(10^4\times\omega_{a,i}\right)\right]^{\frac{1}{2}} - 14.85 \tag{26}$$

To further evaluate the performance of the heat and mass exchanger, the cooling capacity (*CC*) is calculated. Cooling capacity represents the change in air sensible heat across the wet tube channel, and is expressed as follows:

$$CC = \rho_a \cdot A_c \cdot \dot{V}_{a,o} \cdot C_{pa}\left(T_{a,i}-T_{a,o}\right) \tag{27}$$

The specific cooling capacity, defined as the cooling capacity per square meter of exchange surface area, is also used to assess the exchanger's performance. It is expressed as follows:

$$SCC = \frac{\rho_a \cdot A_c \cdot \dot{V}_{a,o} \cdot C_{pa}\left(T_{a,i}-T_{a,o}\right)}{A_w} \tag{28}$$

The water consumption rate (m_e) depends on factors such as inlet/outlet air humidity, and airflow rate. It is calculated using Equation (29):

$$m_e = \rho_a A_c \dot{V}_{a,o}\left(\omega_{a,o}-\omega_{a,i}\right) \tag{29}$$

These equations collectively provide a comprehensive framework to predict the

terracotta tubes' heat and mass exchanger performance and optimize their design. For additional details regarding the integration process, refer to Windnigda *et al.* [29].

3.5. Determination of the Heat and Mass Transfer Coefficients

Calculating the heat transfer coefficient starts with determining the Reynolds number (Re_a) and the Prandtl number (Pr_a) whose expressions are given below [40]:

$$Re_a = \frac{\rho_a v_a D_e}{\mu_a} \tag{30}$$

$$Pr_{av} = \frac{\mu_a c_{pa}}{\lambda_a} \tag{31}$$

These dimensionless numbers are crucial for estimating heat transfer coefficients in convection, representing fluid flow and the balance between momentum and thermal transport. The Reynolds number indicates the flow regime, while the Prandtl number relates viscosity to thermal conductivity. They are used in empirical correlations to calculate the Nusselt number and heat transfer coefficient. Kays [41] developed a correlation for the Nusselt number to estimate the heat transfer coefficient of air during laminar flow ($Re < 2300$) in a duct with a constant wall temperature.

$$Nu_a = 3.66 + \frac{0.104\left(Re_a Pr_a \left(D_e/L\right)\right)}{1+0.016\left(Re_a Pr_a \left(D_e/L\right)\right)^{0.8}} \tag{32}$$

Under turbulent flow regime, Dreyer *et al.* [31] proposed Equation (33):

$$Nu_a = \frac{\frac{f_a}{8}\left(Re_a - 1000\right) Pr_a \left(1+\left(\frac{D_e}{L}\right)^{0.67}\right)}{1+12.7\left(\frac{f_a}{8}\right)^{0.5}\left(Pr_a^{0.67}-1\right)} \tag{33}$$

where the friction factor f_a for smooth tubes was defined as:

$$f_a = \left[1.82\log_{10}\left(Re_a\right) - 1.64\right]^{-2} \tag{34}$$

Equation (33) is valid for the following range:

$$2300 < Re_a < 10^6; 0.5 < Pr_a < 10^4; 0 < D_e/L < 1.$$

The convective heat transfer coefficient is then deduced using Equation (35) [42].

$$h_a = \frac{Nu_a \cdot \lambda_a}{D_e} \tag{35}$$

The mass transfer coefficient (h_m) can similarly be obtained via the Sherwood number (Sh_a) or deduced using the Lewis factor:

$$h_m = \frac{h_a Le^{-\frac{2}{3}}}{\rho_a c_{pav}} \tag{36}$$

3.6. Thermo-Physical Properties of Moist Air

The analytical model employs psychrometric correlation equations from [43] to calculate the thermodynamic properties of moist air, including temperature-dependent specific heat, density, conductivity, and viscosity for dry air, water vapor, and moist air. These equations, derived from theory and numerical fitting, provide reliable expressions for these properties at atmospheric pressure within a temperature range of 220 - 380 K.

3.7. Computer Simulation Procedure

Figure 3 illustrates the computational simulation flowchart.

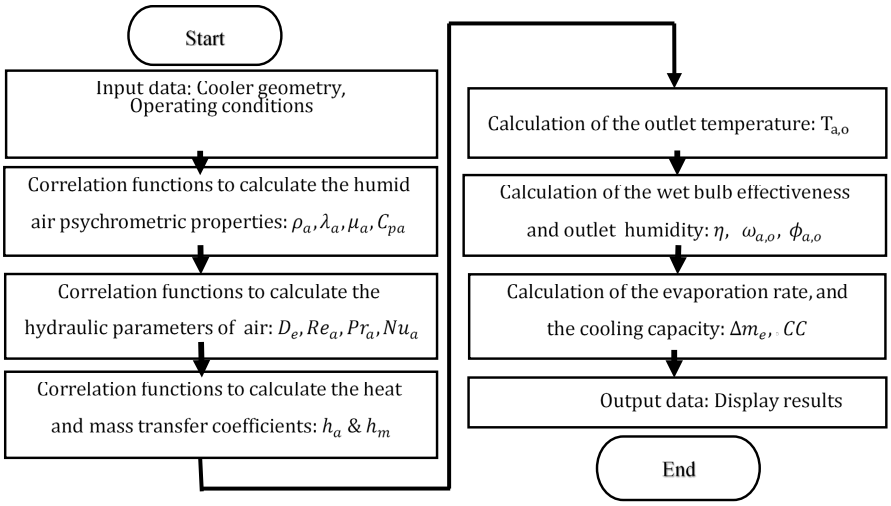

Figure 3. Flowchart of the computational simulation procedure.

3.8. Model Validation

The developed analytical model was validated against numerical results from Kovačević and Sourbron [44], who studied plate-type direct evaporative coolers. Although this study focuses on a terracotta flat tubular configuration, the heat and mass transfer processes are similar to those in plate-type coolers, allowing for comparative validation. To ensure consistency, geometric dimensions such as a 3.4 mm hydraulic diameter and 9 cm tube length, matching those used by Kovačević and Sourbron, were maintained.

4. Results and Discussion

4.1. Validation Results

The validation results in Figure 4 show a strong correlation between the outlet air temperatures predicted by the current model and the numerical model from Kovačević and Sourbron [44], especially across varying inlet air temperatures and humidity levels. The close alignment indicates that the analytical model is effective in simulating the cooling performance of a terracotta tubular heat and mass exchanger, with a minimal discrepancy for inlet air temperatures below 40˚C,

suggesting the model's accuracy in this range. The root mean square deviation (RMSD) remains low overall, though it rises slightly as inlet air humidity increases. This increase in RMSD with humidity may point to limitations in the model's precision under higher temperature and humidity conditions, potentially due to alteration in heat and mass transfer rates not fully captured by the present analytical model. Overall, these comparison results confirm the validity of the proposed model.

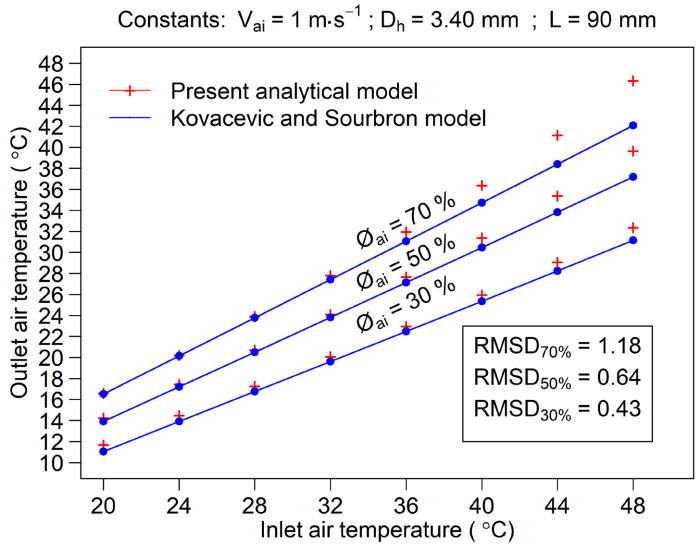

Figure 4. Comparison between our model results with that of Kovačević and Sourbron.

The air treatment performance of the porous terracotta tubular heat and mass exchanger is analyzed using the validated model to examine the impact of key design and operating parameters, including tube flatness, equivalent diameter, inlet air temperature, humidity, and air velocity. By varying these parameters individually while holding others constant, the study evaluates performance metrics such as outlet air temperature, cooling capacity, wet bulb effectiveness, and water evaporation rate. Understanding and optimizing these parameters are essential for enhancing heat and mass transfer characteristics and maximizing cooling performance under diverse environmental conditions and applications.

4.2. Influence of Channel Equivalent Diameter

The channel's equivalent diameter significantly impacts mass flow rate and heat and mass transfer coefficients, influencing the cooling performance of the system. As shown in **Figure 5**, increasing the equivalent diameter (from 10 to 25 mm) reduces air outlet temperature and wet bulb effectiveness (**Figure 5(a)** & **Figure 5(c)**) while enhancing cooling capacity and water consumption rates (**Figure 5(b)** & **Figure 5(d)**). This is due to the improved heat and mass transfer rates with

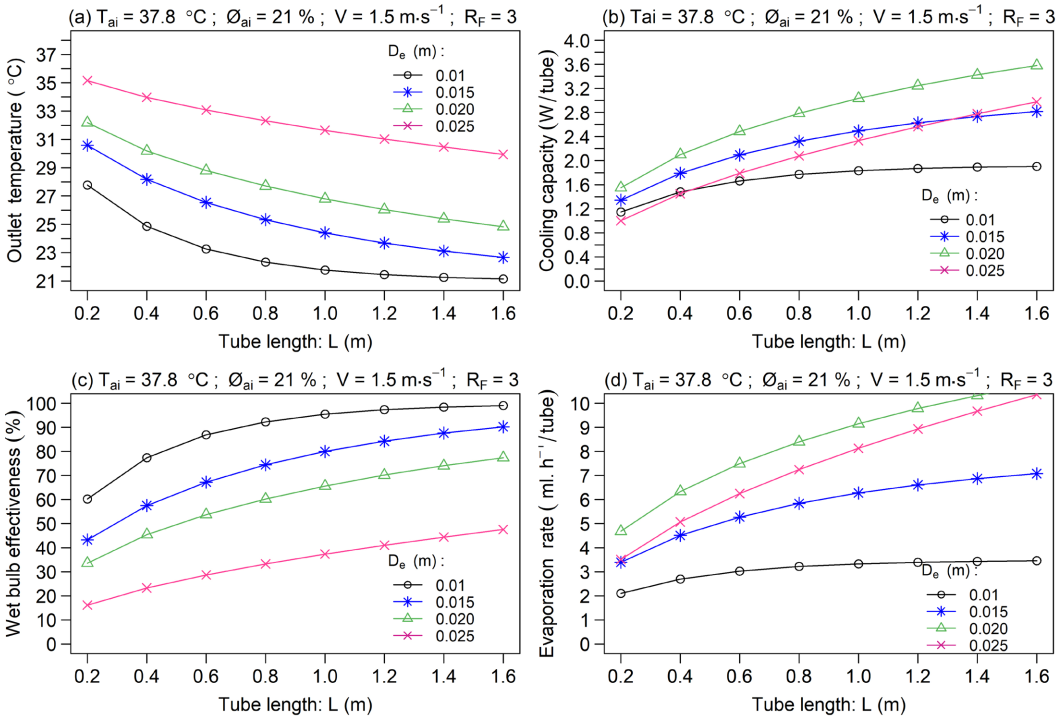

Figure 5. Influence of channel equivalent diameter on the cooling performance parameters.

smaller diameters, which enhance cooling effectiveness but lower cooling capacity due to reduced airflow. Beyond 20 mm, performance declines sharply, suggesting a transition to turbulent flow, which adversely affects the Nusselt number and transfer rates. Tube length also plays a crucial role, with longer tubes improving wet bulb effectiveness and cooling capacity but increasing structural fragility. Optimal diameters range from 5 mm for shorter tubes (<0.5 m) to 10 mm for medium-length tubes (0.5 - 1 m), balancing performance and practical considerations.

4.3. Influence of Tube Flatness Ratio

The tube flatness ratio, defined by the ratio of the tube's long to short axes, significantly influences the cooling performance of the exchanger. As shown in **Figure 6**, increasing the flatness ratio enhances cooling capacity (**Figure 6(b)**), wet bulb effectiveness (**Figure 6(c)**), and reduces air outlet temperature (**Figure 6(a)**), though it also slightly increases water consumption (**Figure 6(d)**). While airflow rate and heat and mass transfer coefficients remain unchanged due to constant air velocity and equivalent diameter, a higher flatness ratio increases the heat exchange surface area, improving heat removal efficiency. For example, at an equivalent diameter of 15 mm and a tube length of 0.6 m, increasing the flatness ratio from 1 (circular) to 4 expands the surface area from 0.028 to 0.037 m^2, boosting wet bulb effectiveness from 60% to 71%. This demonstrates the effectiveness of flat tubes in enhancing heat dissipation and wettability, making them a compact and efficient choice for cooling systems.

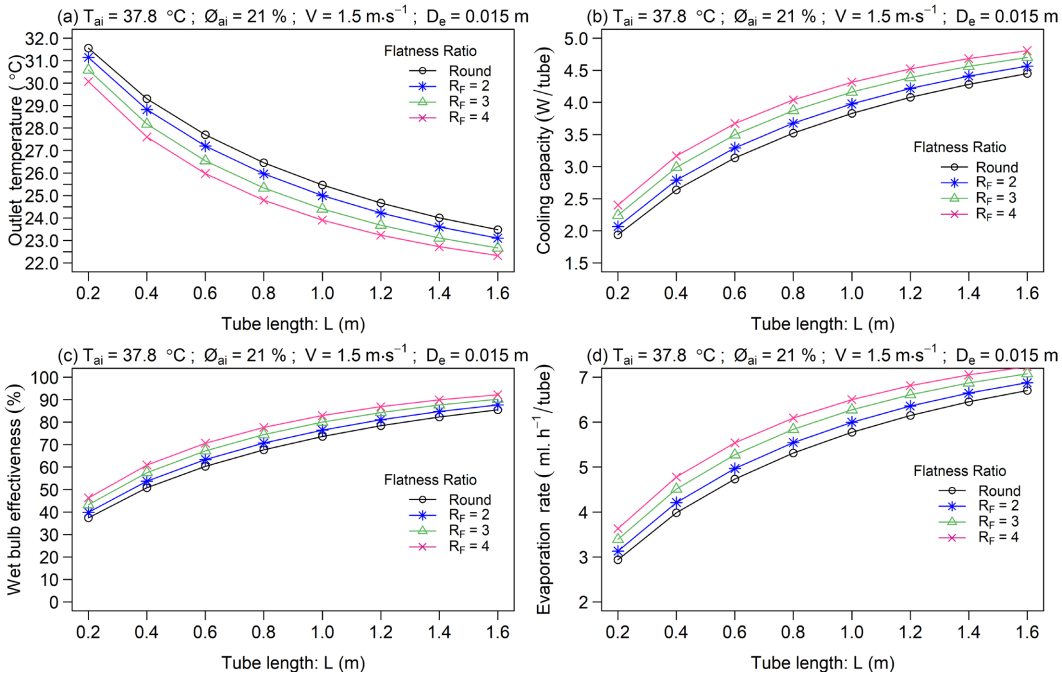

Figure 6. Influence of tube's flatness ratio on the cooling performance parameters.

4.4. Influence of Inlet Air Temperature

This set of simulations examines the effect of inlet air temperature on the cooling performance of the exchanger. **Figure 7** shows that as the inlet air temperature increases, the outlet air temperature (**Figure 7(a)**) and cooling capacity (**Figure 7(b)**) also increase. The rise in cooling capacity with higher inlet air temperatures is due to the increase of the wet bulb depression, which lead to more heat removal from the flowing air. This highlights an advantage of evaporative cooling systems, which improve their cooling capacity under hotter ambient conditions, unlike vapor-compression systems that decline in performance.

Interestingly, **Figure 7(c)** reveals that wet bulb effectiveness remains constant across varying inlet air temperatures, consistent with theoretical predictions that it depends on the exchange surface area, heat/mass transfer coefficient, and air mass flow rate. However, this finding diverges from previous studies (e.g., Kovačević and Sourbron [44]), which reported sensitivity of wet bulb effectiveness to inlet air temperature. This difference likely arises from variations in system configurations and operating conditions. Finally, water consumption rate (**Figure 7(d)**) also increases with rising inlet air temperatures due to the greater evaporation required to achieve cooling.

4.5. Influence of inlet air humidity

Figure 8 illustrates the impact of inlet air relative humidity on the cooling performance of the porous terracotta tube heat and mass exchanger. Results show that increasing inlet air relative humidity raises the outlet air temperature (**Figure 8(a)**) due to higher wet bulb temperatures in humid air, which limit the achievable

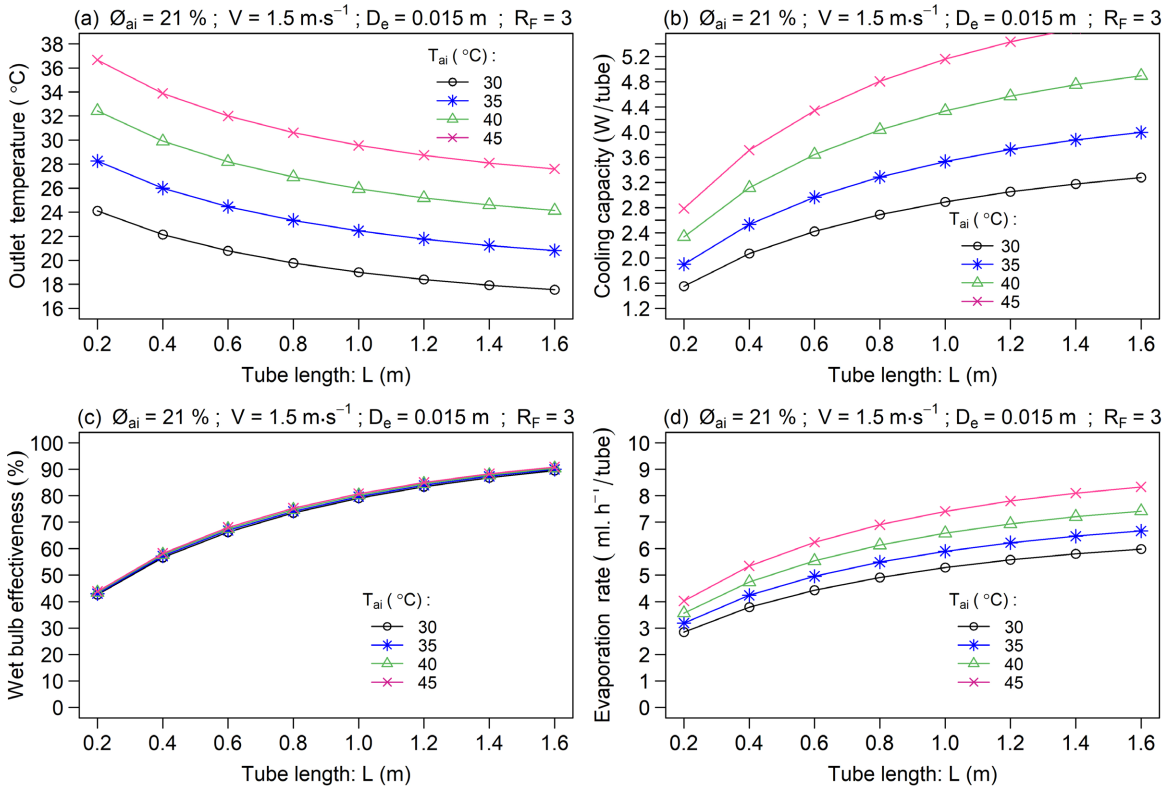

Figure 7. Influence of inlet air temperature on the cooling performance parameters.

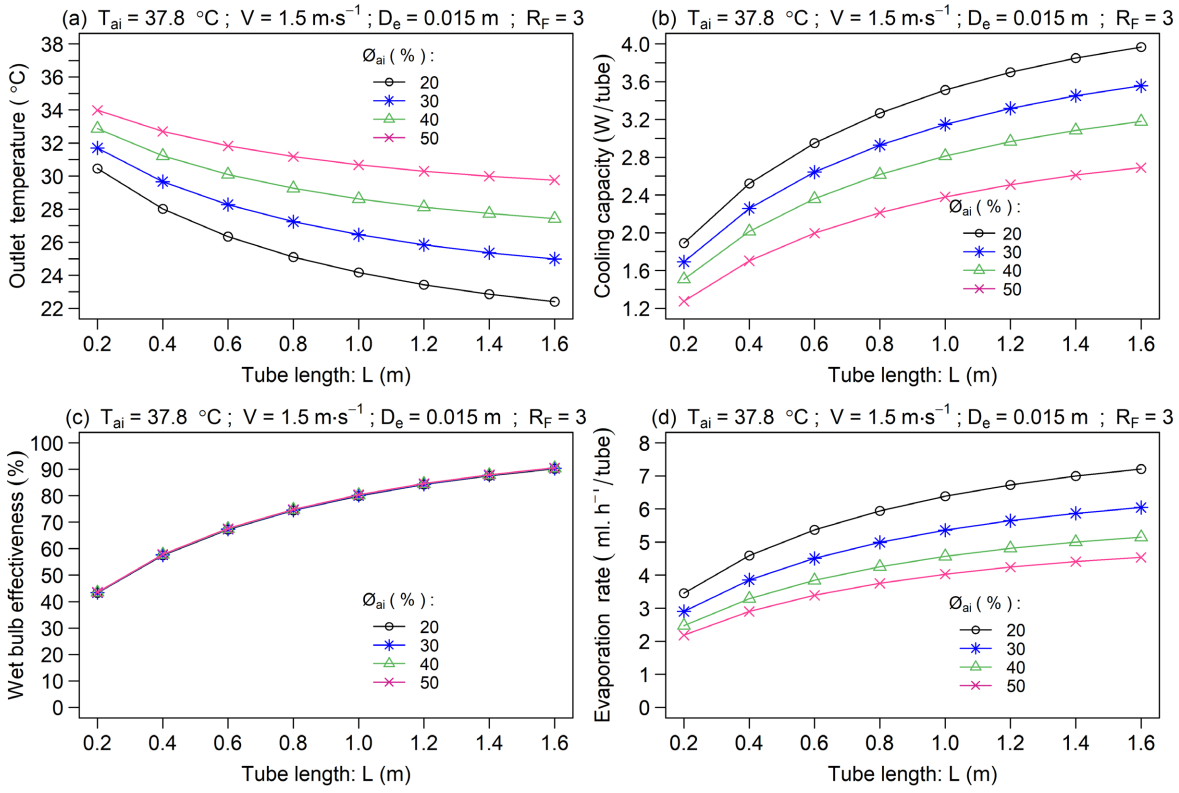

Figure 8. Influence of inlet air relative humidity on the cooling performance parameters.

temperature drop. Cooling capacity (Figure 8(b)) declines with higher relative humidity, as drier air facilitates better moisture absorption and heat removal, enhancing cooling performance. Water consumption rates (Figure 8(d)) are higher at lower relative humidity levels, driven by a greater vapor pressure difference that promotes increased evaporation. In contrast, wet bulb effectiveness (Figure 8(c)) remains unaffected by relative humidity, reaffirming its dependency on design and operational parameters rather than inlet air conditions. These findings highlight the suitability of terracotta-based evaporative cooling systems in arid climates, where low humidity enhances cooling efficiency.

4.6. Effect of Inlet Air Velocity

Figure 9 illustrates the influence of inlet air velocity on the cooling performance of the porous terracotta tube heat and mass exchanger. Increasing air velocity reduces the contact time between air and the wet surface, resulting in a higher outlet air temperature (Figure 9(a)) and lower wet bulb effectiveness (Figure 9(c)). Despite this reduction in cooling effectiveness, higher velocities enhance cooling capacity (Figure 9(b)) by increasing the air volume processed and total heat removed, albeit at the expense of higher water consumption rates (Figure 9(d)). For instance, doubling the air velocity from 1 m/s to 2 m/s decreases wet bulb effectiveness by 20% but increases cooling capacity by 92%. However, exceeding a critical velocity (e.g., 2 m/s) can lead to turbulent flow, diminishing heat and mass transfer efficiency and compromising overall cooling performance. Optimal air

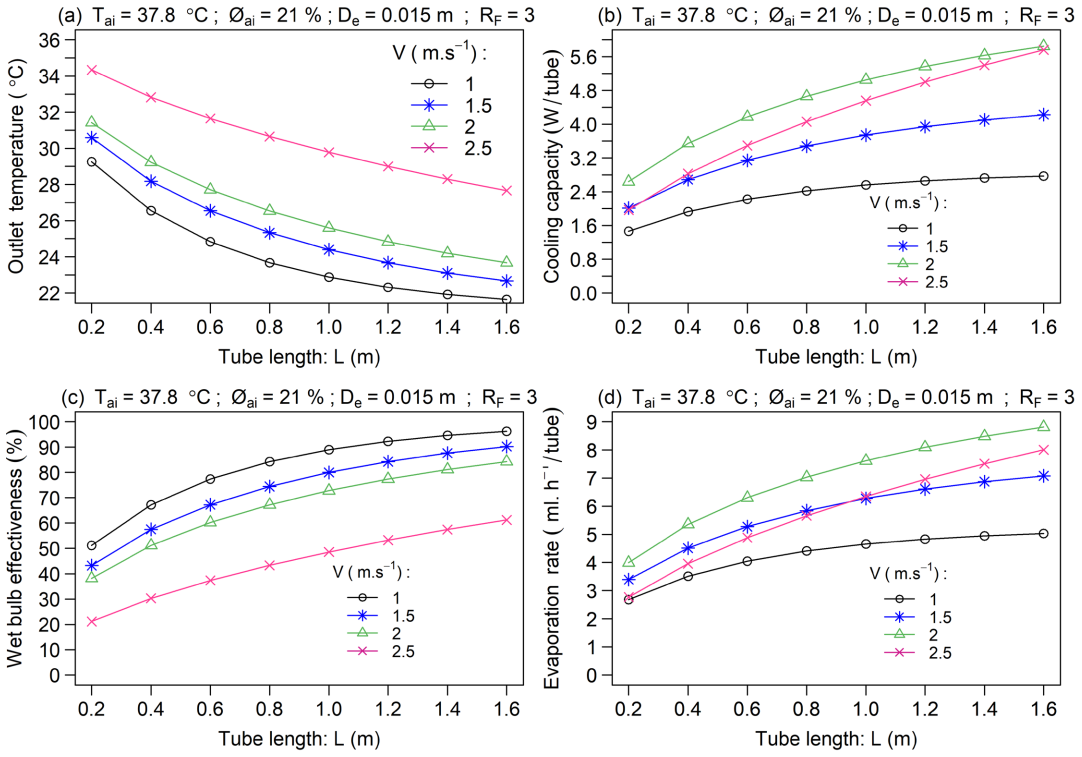

Figure 9. Influence of air velocity on the cooling performance parameters.

velocities depend on tube length: around 1 m/s for tubes under 0.8 m, 1.5 m/s for 0.8 - 1.2 m, and up to 2 m/s for tubes longer than 1.2 m. Adjusting inlet velocity within these ranges ensures a balance between high cooling capacity and thermal comfort while avoiding turbulence.

4.7. Air Temperature and Humidity Distribution along the Wet Channel

The temperature and humidity profiles of the airflow along the wet tube channel, as illustrated in Figure 10, demonstrate complementary trends due to simultaneous heat transfer and water evaporation processes. Air temperature decreases exponentially along the channel as heat is transferred from the warm air to the cooler wet surface, while humidity rises due to evaporation driven by the vapor pressure difference. The latent heat required for evaporation is supplied by thermal energy extracted from the air, highlighting the integrated nature of heat and mass transfer.

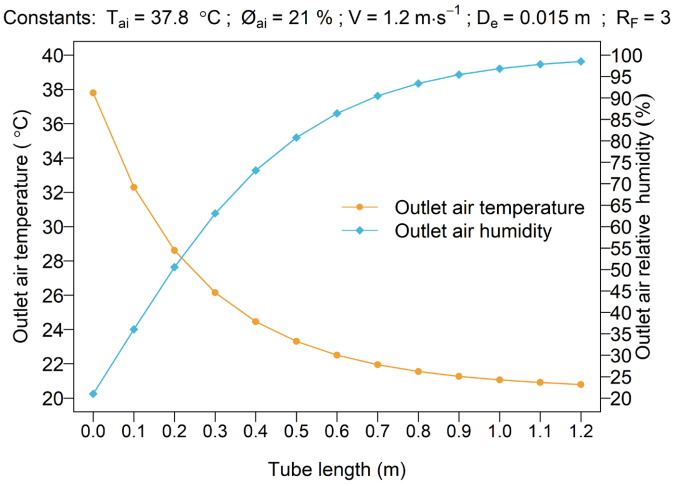

Figure 10. Air temperature and humidity distribution along the tube channel.

5. Conclusion

This paper presents a new analytical model used to simulate the cooling performance of a porous terracotta tubular direct evaporative heat and mass exchanger, offering valuable insights into the effects of design and operational parameters. By integrating energy and mass balance equations with heat and mass transfer coefficients and psychrometric property correlations, the model shows strong agreement with established numerical simulation models. Key findings emphasize the influence of terracotta tube geometry, such as equivalent diameter, flatness ratio, and length, on cooling performance. Smaller diameters enhance wet-bulb effectiveness but reduce overall cooling capacity, while increased flatness and length improve both metrics. The analysis also indicates that under specific design conditions, wet-bulb effectiveness remains unaffected by variations in inlet air

temperature and humidity. Moreover, optimizing air velocity relative to equivalent diameter and tube length is crucial for achieving a balance between cooling capacity and thermal comfort. This analytical model offers a practical and reliable solution for early design of evaporative cooling systems, simplifying complex numerical and CFD methods. Future research may focus on experimental investigation, advanced numerical modeling, and sustainability assessments to enhance performance, accuracy, and feasibility of terracotta-based cooling systems.

Funding

The work described in this paper was supported by a Research Grant from the Federal Ministry of Education and Research of Germany (Grant No. WASCAL_GRP_CCE2).

Conflicts of Interest

The authors declare no conflicts of interest regarding the publication of this paper.

References

[1] Delgado, J.M. (2011) Heat and Mass Transfer in Porous Media. Springer.

[2] Budu, A.R., Pavel, G.L. and Moraru, D.E. (2017) Heat and Mass Transfer Aspects in Nuclear Power Generation. *Energy Procedia*, **112**, 571-578. https://doi.org/10.1016/j.egypro.2017.03.1119

[3] Derby, M.M., Adams, A.N., Chakraborty, P.P., Haque, M.R., Huber, R.A., Morrow, J.A., *et al.* (2020) Heat and Mass Transfer in the Food, Energy, and Water Nexus—A Review. *Journal of Heat Transfer*, **142**, Article ID: 090801. https://doi.org/10.1115/1.4047089

[4] Delfani, S., Esmaeelian, J., Pasdarshahri, H. and Karami, M. (2010) Energy Saving Potential of an Indirect Evaporative Cooler as a Pre-Cooling Unit for Mechanical Cooling Systems in Iran. *Energy and Buildings*, **42**, 2169-2176. https://doi.org/10.1016/j.enbuild.2010.07.009

[5] Wanphen, S. and Nagano, K. (2009) Experimental Study of the Performance of Porous Materials to Moderate the Roof Surface Temperature by Its Evaporative Cooling Effect. *Building and Environment*, **44**, 338-351. https://doi.org/10.1016/j.buildenv.2008.03.012

[6] Zhao, X., Liu, S. and Riffat, S.B. (2008) Comparative Study of Heat and Mass Exchanging Materials for Indirect Evaporative Cooling Systems. *Building and Environment*, **43**, 1902-1911. https://doi.org/10.1016/j.buildenv.2007.11.009

[7] Malli, A., Seyf, H.R., Layeghi, M., Sharifian, S. and Behravesh, H. (2011) Investigating the Performance of Cellulosic Evaporative Cooling Pads. *Energy Conversion and Management*, **52**, 2598-2603. https://doi.org/10.1016/j.enconman.2010.12.015

[8] Shekhar, S., Suman, S., Moharana, H. and Sethy, D. (2016) Performance of Different Pad Materials in Advanced Desert Coolers—A Comparative Study. *International Journal of Engineering Science*, **4368**, 250-254.

[9] Velasco-Gómez, E., Tejero-González, A., Jorge-Rico, J. and Rey-Martínez, F.J. (2020) Experimental Investigation of the Potential of a New Fabric-Based Evaporative Cooling Pad. *Sustainability*, **12**, Article 7070. https://doi.org/10.3390/su12177070

[10] Franco-Salas, A., Peña-Fernández, A. and Valera-Martínez, D.L. (2019) Refrigeration Capacity and Effect of Ageing on the Operation of Cellulose Evaporative Cooling Pads, by Wind Tunnel Analysis. *International Journal of Environmental Research and Public Health*, **16**, Article 4690. https://doi.org/10.3390/ijerph16234690

[11] Abdullah, A. (2022) Experimental Study of Natural Materials for an Evaporative Cooling Design in Hot-Arid Climate. *Building and Environment*, **207**, Article ID: 108564. https://doi.org/10.1016/j.buildenv.2021.108564

[12] He, J. and Hoyano, A. (2010) Experimental Study of Cooling Effects of a Passive Evaporative Cooling Wall Constructed of Porous Ceramics with High Water Soaking-Up Ability. *Building and Environment*, **45**, 461-472. https://doi.org/10.1016/j.buildenv.2009.07.002

[13] Ibrahim, E., Shao, L. and Riffat, S.B. (2003) Performance of Porous Ceramic Evaporators for Building Cooling Application. *Energy and Buildings*, **35**, 941-949. https://doi.org/10.1016/s0378-7788(03)00019-7

[14] Wang, F., Sun, T., Huang, X., Chen, Y. and Yang, H. (2017) Experimental Research on a Novel Porous Ceramic Tube Type Indirect Evaporative Cooler. *Applied Thermal Engineering*, **125**, 1191-1199. https://doi.org/10.1016/j.applthermaleng.2017.07.111

[15] Amer, O. and Boukhanouf, R. (2016) Experimental Investigation of a Novel Heat Pipe and Porous Ceramic Based Indirect Evaporative Cooler.

[16] Herrero Martín, R., Rey Martínez, F.J. and Velasco Gómez, E. (2008) Thermal Comfort Analysis of a Low Temperature Waste Energy Recovery System: SIECHP. *Energy and Buildings*, **40**, 561-572. https://doi.org/10.1016/j.enbuild.2007.04.009

[17] Velasco Gómez, E., Rey Martínez, F.J., Varela Diez, F., Molina Leyva, M.J. and Herrero Martín, R. (2005) Description and Experimental Results of a Semi-Indirect Ceramic Evaporative Cooler. *International Journal of Refrigeration*, **28**, 654-662. https://doi.org/10.1016/j.ijrefrig.2005.01.004

[18] Feng, S. and Liu, Q. (2007) Research of Heat and Mass Transfer Process on Foam Ceramic Fillers Surface. *Contamination Control & Air-Conditioning Technology*, **4**, 11-14.

[19] Chen, W., Liu, S. and Lin, J. (2015) Analysis on the Passive Evaporative Cooling Wall Constructed of Porous Ceramic Pipes with Water Sucking Ability. *Energy and Buildings*, **86**, 541-549. https://doi.org/10.1016/j.enbuild.2014.10.055

[20] Mechergui, O., Chesneau, X. and Laatar, A.H. (2017) Heat and Mass Transfers by Natural Convection during Water Evaporation in a Vertical Channel. *Computational Thermal Sciences: An International Journal*, **9**, 423-445. https://doi.org/10.1615/computthermalscien.2017019798

[21] Kassim, M.A., Benhamou, B. and Harmand, S. (2010) Combined Heat and Mass Transfer with Phase Change in a Vertical Channel. *Computational Thermal Sciences*, **2**, 299-310. https://doi.org/10.1615/computthermalscien.v2.i4.10

[22] Cherif, A.S., Kassim, M.A., Benhamou, B., Harmand, S., Corriou, J.P. and Ben Jabrallah, S. (2011) Experimental and Numerical Study of Mixed Convection Heat and Mass Transfer in a Vertical Channel with Film Evaporation. *International Journal of Thermal Sciences*, **50**, 942-953. https://doi.org/10.1016/j.ijthermalsci.2011.01.002

[23] Cossali, G.E. and Tonini, S. (2019) An Analytical Model of Heat and Mass Transfer from Liquid Drops with Temperature Dependence of Gas Thermo-Physical Properties. *International Journal of Heat and Mass Transfer*, **138**, 1166-1177. https://doi.org/10.1016/j.ijheatmasstransfer.2019.04.066

[24] Adam, A., Han, D., He, W. and Amidpour, M. (2021) Analysis of Indirect Evaporative

Cooler Performance under Various Heat and Mass Exchanger Dimensions and Flow Parameters. *International Journal of Heat and Mass Transfer*, **176**, Article ID: 121299. https://doi.org/10.1016/j.ijheatmasstransfer.2021.121299

[25] Sun, T., Huang, X., Qu, Y., Wang, F. and Chen, Y. (2020) Theoretical and Experimental Study on Heat and Mass Transfer of a Porous Ceramic Tube Type Indirect Evaporative Cooler. *Applied Thermal Engineering*, **173**, Article ID: 115211. https://doi.org/10.1016/j.applthermaleng.2020.115211

[26] Hasan, A. and Sirén, K. (2004) Performance Investigation of Plain Circular and Oval Tube Evaporatively Cooled Heat Exchangers. *Applied Thermal Engineering*, **24**, 777-790. https://doi.org/10.1016/j.applthermaleng.2003.10.022

[27] Chua, K.J., Xu, J., Cui, X., Ng, K.C. and Islam, M.R. (2015) Numerical Heat and Mass Transfer Analysis of a Cross-Flow Indirect Evaporative Cooler with Plates and Flat Tubes. *Heat and Mass Transfer*, **52**, 1765-1777. https://doi.org/10.1007/s00231-015-1696-y

[28] Liu, Z., Quan, Z., Zhao, Y., Jing, H. and Yang, M. (2022) Performance Optimization of Ice Thermal Storage Device Based on Micro Heat Pipe Arrays. *International Communications in Heat and Mass Transfer*, **134**, Article ID: 106051. https://doi.org/10.1016/j.icheatmasstransfer.2022.106051

[29] Windnigda, Z., Makinta, B., Ousmane, C., Christian, T.G. and Antoine, B. (2024) Modeling Heat and Mass Transfer in a Wet Terracotta Tube Channel for Evaporative Cooling Application: Influence of Geometrical Parameters. *Physical Science International Journal*, **28**, 1-20. https://doi.org/10.9734/psij/2024/v28i6855

[30] Sheng, C. and Nnanna, A.G.A. (2011) Empirical Correlation of Cooling Efficiency and Transport Phenomena of Direct Evaporative Cooler. *ASME* 2011 *International Mechanical Engineering Congress and Exposition*, Denver, 11-17 November 2011, 953-967. https://doi.org/10.1115/imece2011-63227

[31] Dreyer, A.A. and Erens, P.J. (1990) Heat and Mass Transfer Coefficient and Pressure Drop Correlations for a Crossflow Evaporative Cooler. *Proceeding of International Heat Transfer Conference* 9, Hemisphere Publishing Company, New York, 233-238. https://doi.org/10.1615/ihtc9.740

[32] Gupta, A.K., Kashyap, S. and Sarkar, J. (2022) Machine Learning Model of Regenerative Evaporative Cooler for Performance Prediction Based on Experimental Investigation. *International Journal of Refrigeration*, **137**, 178-187. https://doi.org/10.1016/j.ijrefrig.2022.02.006

[33] Hosoz, M., Ertunc, H.M. and Ozguc, A.F. (2007) Modelling of a Direct Evaporative Air Cooler Using Artificial Neural Network. *International Journal of Energy Research*, **32**, 83-89. https://doi.org/10.1002/er.1336

[34] Sohani, A., Sayyaadi, H. and Mohammadhosseini, N. (2018) Comparative Study of the Conventional Types of Heat and Mass Exchangers to Achieve the Best Design of Dew Point Evaporative Coolers at Diverse Climatic Conditions. *Energy Conversion and Management*, **158**, 327-345. https://doi.org/10.1016/j.enconman.2017.12.042

[35] Jafarian, H., Sayyaadi, H. and Torabi, F. (2017) Modeling and Optimization of Dew-Point Evaporative Coolers Based on a Developed GMDH-Type Neural Network. *Energy Conversion and Management*, **143**, 49-65. https://doi.org/10.1016/j.enconman.2017.03.015

[36] Cheng, L., Ribatski, G., Wojtan, L. and Thome, J.R. (2006) New Flow Boiling Heat Transfer Model and Flow Pattern Map for Carbon Dioxide Evaporating Inside Horizontal Tubes. *International Journal of Heat and Mass Transfer*, **49**, 4082-4094. https://doi.org/10.1016/j.ijheatmasstransfer.2006.04.003

[37] Ambaum, M.H.P. (2020) Accurate, Simple Equation for Saturated Vapour Pressure over Water and Ice. *Quarterly Journal of the Royal Meteorological Society*, **146**, 4252-4258. https://doi.org/10.1002/qj.3899

[38] Joudi, K.A. and Mehdi, S.M. (2000) Application of Indirect Evaporative Cooling to Variable Domestic Cooling Load. *Energy Conversion and Management*, **41**, 1931-1951. https://doi.org/10.1016/s0196-8904(00)00004-2

[39] Watt, J.R. and Brown, K.B. (1997) Evaporative Air Conditioning Handbook. 3rd Edition, Chapmann and Hall.

[40] Chinenye, N. and Manuwa, S. (2015) Heat Transfer Coefficient and Concept of Relaxation Time in Forced Air Direct Evaporative Cooling System. *Poljoprivredna Tehnika*, **39**, 99-113.

[41] Kays, W.M. (1955) Numerical Solutions for Laminar-Flow Heat Transfer in Circular Tubes. *Journal of Fluids Engineering*, **77**, 1265-1272. https://doi.org/10.1115/1.4014661

[42] Heidarinejad, G. and Moshari, S. (2015) Novel Modeling of an Indirect Evaporative Cooling System with Cross-Flow Configuration. *Energy and Buildings*, **92**, 351-362. https://doi.org/10.1016/j.enbuild.2015.01.034

[43] Dreyer, A.A. (1988) Analysis of Evaporative Coolers and Condensers. Ph.D. Thesis, Stellenbosch University, Stellenbosch. http://scholar.sun.ac.za

[44] Kovačević, I. and Sourbron, M. (2017) The Numerical Model for Direct Evaporative Cooler. *Applied Thermal Engineering*, **113**, 8-19. https://doi.org/10.1016/j.applthermaleng.2016.11.025

Nomenclature

a	Tube short axis (m)
A_c	Cross−section area (m^2)
A_w	Exchange surface area (m^2)
b	Tube long axis (m)
CC	Cooling Capacity (W)
C_{pa}	Specific heat of air ($J \cdot kg^{-1} \cdot K^{-1}$)
C_{pv}	Specific heat of water vapor ($J \cdot kg^{-1} \cdot K^{-1}$)
D_e	Tube equivalent diameter (m)
D_h	Tube hydraulic diameter (m)
h_a	Heat transfer coefficient ($W \cdot m^{-2} \cdot K^{-1}$)
h_m	Mass transfer coefficient ($m \cdot s^{-1}$)
i_{fg}	Latent heat of vaporization ($J \cdot kg^{-1}$)
L	Tube length (m)
L_e	Lewis number
m_a	Mass flow rate of air ($kg \cdot s^{-1}$)
p	Channel perimeter (m)
P	Pressure (Pa)
T	Temperature (°C)
v	Velocity ($m \cdot s^{-1}$)
m_e	Water consumption rate (m^3/s)
Dimensionless numbers	
Nu	Nusselt number
Pr	Prandtl number
Re	Renold number
R_F	Tube Flatness Ratio
Sc	Schmidt number
Sh	Sherwood number

Greek Letters

ρ	Density ($kg \cdot m^{-3}$)
ω	Specific humidity ($kg_{vapor} \cdot kg_{air}^{-1}$)
Φ	Relative humidity (%)
μ	Dynamic viscosity ($N \cdot s \cdot m^{-2}$)
λ	Thermal conductivity ($W \cdot m^{-1} \cdot K^{-1}$)
ε	Wet bulb effectiveness (%)
η	Saturation efficiency (%)

Subscripts

a	Air
atm	Atmospheric
sat	Saturated
v	Vapor
vs	Saturated water vapor
wb	Wet bulb